THE ASTROPHYSICAL JOURNAL, 542:L131–L133, 2000 October 20

THE ORBIT OF THE BINARY X-RAY PULSAR 4U 1538−52 FROM *ROSSI X-RAY TIMING EXPLORER* OBSERVATIONS

GEORGE W. CLARK
Center for Space Research, 70 Vassar Street, Building 37, Massachusetts Institute of Technology, Cambridge, MA 02139
Received 2000 April 5; accepted 2000 August 24; published 2000 September 29

ABSTRACT

Improved orbital parameters of the high-mass binary X-ray pulsar 4U 1538−52 have been derived from high count rate data obtained from the *Rossi X-Ray Timing Explorer*. Pulse-timing analysis yields an eccentricity of 0.174 ± 0.015, a periastron at $64° \pm 9°$, and evidence of orbital decay with $P_{\rm orb}/P_{\rm orb} = (-2.9 \pm 2.1) \times 10^{-6}$ yr^{-1}.

Subject headings: binaries: eclipsing — pulsars: individual (4U 1538−52) — X-rays: stars

1. INTRODUCTION

The accretion-powered high-mass X-ray pulsar 4U 1538−52 (hereafter X1538) and its B0 I companion QV Nor comprise an eclipsing binary system exhibiting several interesting features that were revealed in previous observations by the *Ginga* X-ray observatory: the spectrum has a pulse-phase–dependent feature around 20 keV that was identified as an effect of the cyclotron resonance on the Compton scattering in the accretion columns of the neutron star (Clark et al. 1990); the X-ray image has a prominent grain-scattered halo that exhibits the effects of travel-time differences on its decay when the central source is eclipsed (Clark, Woo, & Nagase 1994); and pulse-timing analysis yielded evidence of orbital eccentricity with a value of 0.082 ± 0.047 (Corbet, Woo, & Nagase 1993). Optical observations of the velocity curve of QV Nor, combined with previously determined orbital parameters of X1538, yielded a mass of $19.8 \pm 3.3\ M_\odot$ for the companion star (Reynolds, Bell, & Hilditch 1992).

This Letter describes new measurements of the orbital parameters of X1538 derived from pulse-timing analysis of high count rate data from the *Rossi X-Ray Timing Explorer* (*RXTE*). The results show a surprisingly large eccentricity and evidence of orbital decay.

2. OBSERVATIONS AND DATA REDUCTION

The observations occurred in 1997 during January 1.93–5.69 UT (MJD 50,449.93–50,453.69) with a total useful exposure of 139,723 s, extending from the binary orbital phase 0.93 over one complete orbital period. The *RXTE* observatory has been described by Bradt, Rothschild, & Swank (1993). It has five proportional counter arrays (PCAs) with a total sensitive area of 7000 cm^2, a collimated field of view with a FWHM of 1°, and a nominal energy range extending from 2 to 60 keV. The raw data used in this analysis consist of the arrival time and pulse height of each event detected in the top two layers of the PCAs with a time resolution of 1 ms. The data were processed to obtain the count rates in 1 s intervals tagged with barycentrically corrected times.

3. ORBIT ANALYSIS AND PULSE FREQUENCY

Forty average pulse profiles were formed by epoch-folding the count rates into 80 bins of pulse phase. Each profile was derived from a nearly continuous segment of data spanning approximately 1% of the binary period. Pulse phases were computed for trial values of the intrinsic pulse frequency ν, its rate of change $\dot{\nu}$, and predicted delays in pulse arrival times derived by the solution of the Keplerian equation for trial values of the period $P_{\rm orb}$, epoch $T_{\pi/2}$ (time of mean longitude = 90°), projected semimajor axis $a_x \sin i$, eccentricity e, and periastron ω of an elliptical orbit. A 10-term Fourier series was fitted to a template pulse derived from a continuous segment of data that was free of any substantial flare activity and extending from 120,000 to 134,000 s from the start of the observation. The Fourier representation of the template was cross-correlated with each of the 80 bin profiles, and the relative phase shift of each profile that was due to errors in the trial values was determined by a parabolic interpolation between the phase bin of maximum correlation and its immediate neighbors on either side. The predicted delay at the midtime of the segment was corrected according to these phase shifts in order to obtain a set of measured delays. A curve of predicted delay was then fitted by least squares to the set of measured delays in a two-step procedure by an adjustment of the frequency and orbital parameters with the Levenberg-Marquardt algorithm (Press et al. 1986). In both steps, $P_{\rm orb}$ was fixed at the value determined as described below. In the first step, $\dot{\nu}$ was fixed at zero. In the second step, $a_x \sin i$ was fixed at the fitted value from the first step, and $\dot{\nu}$ was allowed to vary. This two-step procedure was necessary because a fit with both $a_x \sin i$ and $\dot{\nu}$ free to vary was not adequately constrained by the data and yielded absurd values of ν, $\dot{\nu}$, and the orbital parameters.

Four profiles with measured delays that deviated widely from the fitted curves of predicted delays were eliminated, two with low count rates that precluded accurate delay measurements from just before and just after the X-ray eclipse and two with large distortions in shape from intervals containing high flare intensities at orbital phases 0.17 and 0.42.

Errors of the measured delays due to counting statistics were negligible compared with errors caused by variations in the intrinsic shapes of the profiles. To quantify these errors, a constant error σ_p was assigned to each of the delays and adjusted in magnitude to achieve $\chi^2_\nu = 1$ in the second step of the fitting procedure. The adjusted value of σ_p is a measure of both the errors of the measured delays and the quality of the fit.

A quadratic function of orbit number N was fitted to the set of all previous orbital epochs derived by pulse-timing analysis together with the present one. Mideclipse times estimated from observations of eclipse ingress and egress were not included because of their large uncertainties caused by the variable attenuation of the X-rays along the line of sight in circumsource matter near the times of eclipse transitions. The improved value

TABLE 1

PARAMETERS OF THE 4U 1538−52/QV NOR BINARY SYSTEM[a]

Parameter	Elliptical Orbit	Circular Orbit
$a_x \sin i$ (lt-s)	56.6 ± 0.7	54.3 ± 0.6
$T_{\pi/2}$ (MJD)	5,0450.206 ± 0.014	50,450.203 ± 0.009
$P_{\rm pulse}$ (s)	528.809 ± 0.008	528.754 ± 0.005
$\dot{\nu}_{\rm pulse}$ (Hz s^{-1})	$(-0.4 \pm 2.3) \times 10^{-13}$	$(10.2 \pm 1.7) \times 10^{-13}$
e	0.174 ± 0.015	
ω (deg)	64 ± 9	
χ^2_ν (σ_p = 2.27 s)	1.00	3.29
a_0 (MJD)[b]	47,221.488 ± 0.015	
a_1 (days)[b]	3.728366 ± 0.000032	
a_2 (days)[b]	$(-5.5 \pm 4.0) \times 10^{-8}$	
$\dot{P}_{\rm orb}/P_{\rm orb}$ (yr^{-1})	$(-2.9 \pm 2.1) \times 10^{-6}$	

[a] Epoch = MJD 50,449.93400.
[b] $T_{\pi/2}(N) = a_0 + a_1 N + a_2 N^2$.

of the current orbital period computed from the fitted quadratic was used together with the other fitted parameters in a new set of epoch folds to sharpen the template and the average pulse profiles.

This entire process was repeated several times until a final value of $\sigma_p = 2.27$ s was obtained. The resulting values of the orbital parameters are listed in Table 1 with 1 σ errors derived from the diagonal elements of the error matrices. The final set of measured delays and the fitted curve are plotted against time from $T_{\rm start}$ = MJD 50,449.93400 in Figure 1*a*. The deviations are plotted below.

The orbital epochs are listed in Table 2, and their deviations from a fitted linear function of orbit number are displayed in Figure 2 together with the fitted quadratic curve. For the linear fit, $\chi^2_\nu = 0.79$. The quadratic fit has $\chi^2_\nu = 0.56$ and gives $\dot{P}_{\rm orb}/P_{\rm orb} = (-2.9 \pm 2.1) \times 10^{-6}$ yr^{-1}. The low values of χ^2_ν indicate that some of the errors attributed to the epochs were overestimated.

Figure 1*b* displays the delay curve and deviations for a circular orbit ($e = 0$) fitted in the same manner to the same set of measured delays. With $\sigma_p = 2.27$ s, the circular fit had $\chi^2_\nu = 3.29$. The fitted parameters for the circular orbit are listed in Table 1.

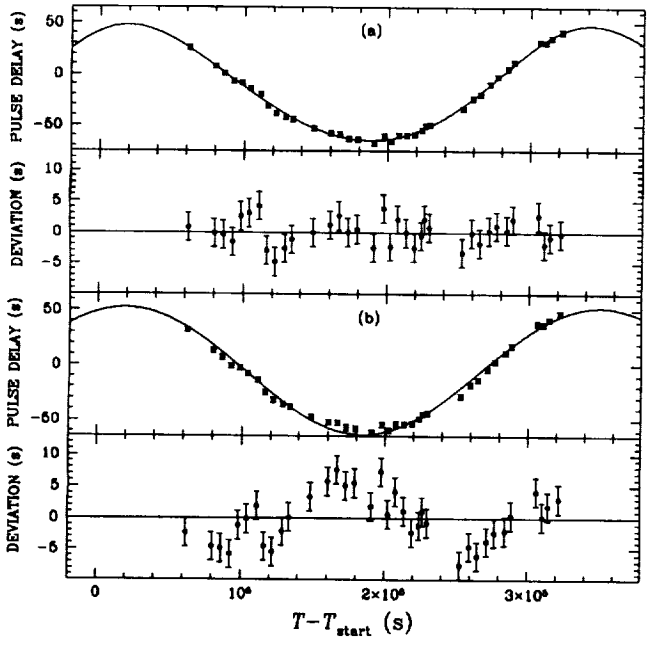

FIG. 1.—Observed delays in pulse arrival times and the fitted arrival time delay curves (*a*) for an elliptical orbit and (*b*) for a circular orbit. The fitted orbital parameters are listed in Table 1.

4. DISCUSSION

The systematic wave of the deviations of the measured delays from the circular fit and the superior quality of the elliptical fit are evidence of a substantial eccentricity of the X1538 orbit. However, the value obtained is surprisingly large for a close binary system in which tidal friction is expected to cause rapid circularization. It is well outside the 95% confidence upper limit of $e = 0.058$ derived by Rubin et al. (1997) from observations by the BATSE instrument on the *Compton Gamma Ray Observatory* and substantially larger than the value found by Corbet et al. (1993). The BATSE upper limit may be in error because of the difficulties inherent in the analysis of data with a very low signal-to-noise ratio recorded over many orbital periods during which fluctuations and the secular variation of the pulse frequency occurred. The BATSE analysis did yield a value of $a_x \sin i = 53.5 \pm 1.4$ lt-s that is consistent with the value found here for the circular orbit fit. Nevertheless, the question arises as to whether the eccentricity found here as well, perhaps, as that found previously in the *Ginga* data could be artifacts of fluctuations in pulse frequency like those revealed in the BATSE study.

In the BATSE observations, the pulse frequency was measured at 16 day intervals over 1600 days. Rubin et al. (1997) found that the power density spectrum of the frequency derivative fluctuations was approximately flat over the range of sampling frequencies from 5×10^{-9} to 3.6×10^{-7} Hz s^{-1} with an rms noise level of $S = (7.6 \pm 1.6) \times 10^{-21}$ (Hz s^{-1})^2 Hz^{-1}. They found that the observed frequency history could be ac-

TABLE 2

EPOCHS MEASURED BY PULSE-TIMING ANALYSIS

Source	Orbit Number	Epoch (MJD)	Error	Reference
OSO 8	−1128	43,015.800	0.100	Becker et al. 1977
Tenma	−457	45,517.660	0.050	Makishima et al. 1987
Ginga	0	47,221.474	0.020	Corbet et al. 1993
BATSE	370	48,600.979	0.027	Rubin et al. 1997
	478	49,003.629	0.022	Rubin et al. 1997
	584	49,398.855	0.029	Rubin et al. 1997
	691	49,797.781	0.022	Rubin et al. 1997
RXTE	866	50,450.206	0.014	Present work

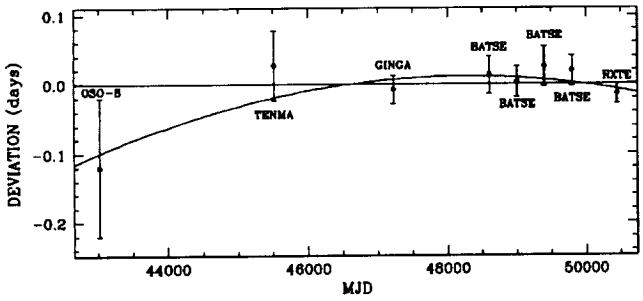

FIG. 2.—Differences between the epochs measured by pulse-timing analysis and the epochs predicted by a fitted linear function of orbit number. The curve is a plot of the differences between a quadratic function of orbit number fitted to the measured epochs and the linear prediction. The coefficients of the quadratic function are listed in Table 1.

counted for as a random walk in pulse frequency with a step size equal to a Gaussian variate with a zero mean and standard deviation $(S\Delta t)^{1/2}$, where Δt is the time interval between steps that they set equal to one orbital period, ~1/4.3 of the shortest sampling interval of their frequency derivative measurements.

We explored the possible effects on our determination of orbital parameters of a similar random walk in frequency, assuming the same rms noise level to be valid for the even shorter time intervals between our delay measurements. Sets of 36 artificial delays with random walk deviations were generated at the times of the observed delays. Specifically, to each exact delay computed at time t_i for a given orbit, we added a deviation

$$\Delta D_i = \sum_{j=1}^{j=i} \delta D_j + e_i, \quad (1)$$

where

$$\delta D_j = \left(\sum_{k=1}^{j-1} \delta\nu_k + \frac{\delta\nu_j}{2}\right)(t_j - t_{j-1})P_{\rm pulse}, \quad j = 2, \ldots, 36. \quad (2)$$

Here e_i represents the random measurement error computed as a Gaussian variate with zero mean and a standard deviation equal to 2.27 s, $\delta D_1 = 0$, $\delta\nu_1 = 0$, $\delta\nu_{j>1}$ is a Gaussian variate with zero mean and a standard deviation equal to $[S(t_j - t_{j-1})]^{1/2}$, and $P_{\rm pulse}$ is the pulse period.

One thousand sets of delays generated for a circular orbit with $a_x \sin i = 56.6$ lt-s were fitted with elliptical orbits as previously described. The rms frequency excursion was 4.47×10^{-8} Hz, close to the expectation value of 4.44×10^{-8} Hz for the time interval of 259,740 s between the first and last delay measurements. The rms delay excursion was 3.60 s, close to the expectation value of 3.05 s if each frequency excursion had occurred at a constant rate of change. The mean values and rms deviations of the results were $\chi^2_\nu = 1.02 \pm 0.26$, $e = 0.033 \pm 0.018$, $a_x \sin i = 56.65 \pm 1.06$ lt-s, $\dot\nu = (0.058 \pm 0.744) \times 10^{-13}$ Hz s^{-1}, and $T_{\pi/2}$ = MJD 50,450.207 ± 0.015. The values of ω were distributed from 0° to 360°, as expected. The largest e in the 1000 trials was 0.10. The value of e derived from the real data is larger than its mean in the test sample by 7.8 times its rms deviation from the mean. Thus, it appears very unlikely that the eccentricity derived from the *RXTE* data is an artifact of random frequency derivative fluctuations, with the noise level found in the BATSE data.

Previous measurements of change in the orbital period of X1538 have yielded values with 1 σ error ranges that include zero. The value found here, $(-2.9 \pm 2.1) \times 10^{-6}$ yr^{-1}, lies within the 95% confidence range of $-3.9 < \dot P_{\rm orb}/P_{\rm orb} < 2.1$ in units of 10^{-6} yr^{-1} derived from the BATSE data (Rubin et al. 1997) and is within a factor of 2 of the orbital decay rates that have been measured in Cen X-3 (Nagase et al. 1992), SMC X-1 (Levine et al. 1993), and 4U 1700−37 (Rubin et al. 1996).

The gross properties of X1538/QV Nor are similar to those of the binary pulsar SMC X-1/Sk 160 (see Levine et al. 1993). Both systems have a highly magnetized neutron star accreting matter from a massive B0 companion in an orbit with nearly the same period and rate of decay. However, X1538/QV Nor is clearly in an earlier stage of evolution. Whereas the orbit of SMC X-1 is highly circular, with a 2 σ upper limit of 4×10^{-5} on its eccentricity, that of X1538 is substantially eccentric. And whereas SMC X-1 draws its huge luminous power by accretion from a relatively stable precessing accretion disk (Wojdowski et al. 1998), X1538 evidently accretes primarily from the stellar wind of its companion and has a much lower X-ray luminosity. Driven by a steady inflow of angular momentum from its accretion disk, SMC X-1 has a high and monotonically increasing spin rate of 1.4 Hz. Driven by inflows of angular momentum that flip in sign on timescales that may be as short as one orbital period or less, X1538 spins up and down erratically around values close to 0.0019 Hz. The decay and circularization of the orbit and evolution of QV Nor will presumably bring a time when accretion occurs through a stable accretion disk fed by Roche lobe overflow, resulting in rapid monotonic spin-up like that observed in SMC X-1.

The author thanks J. Woo for early collaborations in the planning and analysis of these observations and A. Levine, S. Rappaport, and D. Chakrabarty for valuable discussions. Thanks also to a referee for suggested improvements. Data for this study were downloaded from the HEASARC facility of the Goddard Space Flight Center. The help of the HEASARC staff in the data reduction is gratefully acknowledged. This work was supported by NASA under contract NAG5-4485.

REFERENCES

Becker, R. H., Swank, E. A., Boldt, E. A., Holt, S. S., Pravdo, S. H., Saba, J. R., & Serlemitsos, P. J. 1977, ApJ, 216, L11
Bradt, H. V., Rothschild, R. E., & Swank, J. H. 1993, A&AS, 97, 355
Clark, G. W., Woo, J., & Nagase, F. 1994, ApJ, 422, 336
Clark, G. W., Woo, J. W., Nagase, F., Makishima, K., & Sakao, T. 1990, ApJ, 353, 274
Corbet, R. H. D., Woo, J. W., & Nagase, F. 1993, A&A, 276, 52
Levine, A., Rappaport, S., Deeter, J. E., Boynton, P. E., & Nagase, F. 1993, ApJ, 410, 328
Makishima, K., Koyama, K., Hayakawa, S., & Nagase, F. 1987, ApJ, 314, 619
Nagase, F., Corbet, R. H. D., Day, C. S. R., Inoue, H., Takeshima, T., & Yoshida, K. 1992, ApJ, 396, 147
Press, W. H., Flannery, B. P., Teukolsky, S. A., & Vetterling, W. T. 1986, Numerical Recipes (Cambridge: Cambridge Univ. Press)
Reynolds, A. P., Bell, S. A., & Hilditch, R. W. 1992, MNRAS, 256, 631
Rubin, B. C. et al. 1996, ApJ, 459, 259
Rubin, B. C., Finger, M. H., Scott, D. M., & Wilson, R. B. 1997, ApJ, 488, 413
Wojdowski, P., Clark, G. W., Levine, A. M., Woo, J. W., & Zhang, S. N. 1998, ApJ, 502, 253